



Deep-blue thermally activated delayed fluorescence dendrimers with reduced singlet-triplet energy gap for low roll-off non-doped solution-processed organic light-emitting diodes



Jie Li ^{a, b, *}, Xiaoqing Liao ^c, Huixia Xu ^{a, b}, Lu Li ^{c, **}, Jie Zhang ^{a, b}, Hua Wang ^{a, b}, Bingshe Xu ^{a, b}

^a Key Laboratory of Interface Science and Engineering in Advanced Materials, Taiyuan University of Technology, Taiyuan, 030024, China

^b Research Center of Advanced Materials Science and Technology, Taiyuan University of Technology, Taiyuan, 030024, China

^c Co-innovation Center for Micro/Nano Optoelectronic Materials and Devices, Research Institute for New Materials Technology, Chongqing University of Arts and Science, Chongqing, 402160, China

ARTICLE INFO

Article history:

Received 5 December 2016

Received in revised form

14 January 2017

Accepted 15 January 2017

Available online 16 January 2017

Keywords:

TADF

Deep-blue light emitting

Dendrimer

Non-doped

ABSTRACT

Two TADF dendrimers composed of diphenylsulfone core and oligo-carbazole dendrons were developed. Compared with the reported small molecular TADF emitter bis[4-(3,6-di-*tert*-butylcarbazole)phenyl] sulfone (**G1**), dendrimers **G2** and **G3** inherited the blue light emission but exhibited a reduced singlet-triplet energy gap (ΔE_{ST}) with increasing the dendron generation. The efficient triplet-to-singlet (T_1 -to- S_1) transition processes, excellent thermal and amorphous stabilities, good solution processability, and appropriate HOMO/LUMO energy levels enabled these dendrimers to serve as non-doped emitting layers for solution-processed OLEDs. The **G2** device achieved deep-blue light with emission peak at 428 nm, a CIE coordinate at (0.15, 0.12) and relatively low efficiency roll-off at high current density.

© 2017 Elsevier Ltd. All rights reserved.

1. Introduction

Organic light emitting diodes (OLEDs) have attracted much interest due to their applications in the new generation of flat-panel display and solid-state lighting. Among the three primary colors, the development of efficient blue emitters is of high significance for realizing full color displays and white OLEDs for solid-state lighting applications [1–3]. However, the efficiency and stability of blue emitting materials (CIE_y coordinate < 0.15) are still lower than the red and green counterparts [4,5]. The development of deep blue emitters is especially challenging because of their intrinsic wide band gaps, unbalanced carrier transport ability, and poor matching of the energy levels with other functional layers of the OLEDs [6–8]. Among the various design strategies for novel blue emitting materials, thermally activated delayed fluorescence (TADF) materials have becoming promising new generations because of potentially

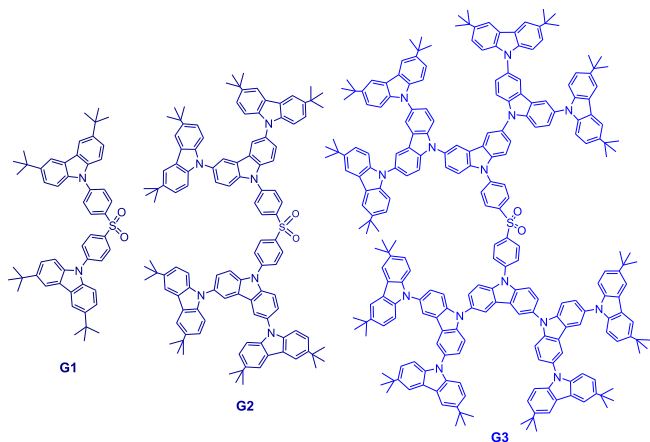
100% internal quantum efficiency by harvesting triplet excitons through a reverse intersystem crossing process [9–11]. Very recently, several highly efficient blue TADF emitters based on diphenylsulfone acceptor were reported by Adachi and coworkers [11–13]. In particular, bis[4-(3,6-di-*tert*-butylcarbazole)phenyl] sulfone (**G1**) demonstrated deep-blue emission and the OLED with this dopant achieved a high EQE of 10% (Scheme 1) [12]. However, the OLED suffered from efficiency roll-off at high current density, which was primarily caused by the relatively large energy gap between the S_1 and T_1 states (ΔE_{ST}). On the other hand, the reported blue TADF emitters are small molecules, which have to be doped into some host materials to suppress emission quenching in the devices [14–16]. For the deep-blue emitters, the use of the host material with a larger energy gap often means inefficient hole and/or electron injection into the emitting layer [17]. Moreover, such doped devices require precise control of the doping concentration, rather complicated structure, and high fabrication costs. As a result, developing efficient blue TADF emitters with solution processability and reduced ΔE_{ST} values for non-doped device is of important significance.

As one of the impressive materials for the non-doped emissive layer, dendrimers exhibit great advantages owing to their well-

* Corresponding author. Key Laboratory of Interface Science and Engineering in Advanced Materials, Taiyuan University of Technology, Taiyuan, 030024, China.

** Corresponding author.

E-mail addresses: lijie01@tyut.edu.cn (J. Li), lli@cqwu.edu.cn (L. Li).



Scheme 1. Molecular structures of TADF dendrimers.

defined structure, controllable molecular size, as well as the inhibited molecular interactions [18,19]. TADF dendrimers displaying green and greenish-blue emission have been utilized for the non-doped solution-processed OLEDs and exhibited satisfying electroluminescent performance [20–23]. However, until now, the reported blue TADF dendrimers are still rare [21], and the relationship between the dendron generation and the S_1 - T_1 energy gap of the molecule, and further the non-doped device performance are still unclear.

In this paper, we report blue TADF dendrimers **G2** and **G3** based on **G1** molecular skeleton as non-doped emissive layers for OLEDs. The density functional theory (DFT) calculation on conformer optimization reveals that 1) the bulky carbazole dendrons lead to three-dimensional molecular conformations and 2) the spatially distribution of the highest occupied molecular orbital (HOMO) and lowest unoccupied molecular orbital (LUMO) of the molecule are related to the generation of the dendrons. Thus, inhibited intermolecular interactions, adjustable ΔE_{ST} of the molecule and further reduced efficiency roll-off of the non-doped device can be anticipated by adjusting the π -conjugation length of the carbazole dendrons. Here, the thermal, photophysical, and electrochemical properties of these dendrimers were systematically investigated. Efficient deep-blue OLEDs with low efficiency roll-off at high current density have been achieved.

2. Experimental section

2.1. Materials and reagents

Unless otherwise indicated, all reagents were purchased from commercial resources and used without further purification. Carbazole was recrystallized from acetone before use. Sodium hydride (60% dispersion in mineral oil) was washed by petroleum ether, dried by ether before use. All air-sensitive reactions were carried out under nitrogen.

2.2. Characterization

The NMR spectra were measured on a Bruker DRX 600 spectrometer, and chemical shifts were reported in ppm using tetramethylsilane as an internal standard. Mass spectra were obtained on a Bruker autoflex MALDI-TOF mass spectrometer. Elemental analysis (EA) was performed by determined with an Vario EL elemental analyzer. The UV–visible absorption spectra were determined on a Hitachi U-3900 spectrophotometer. The

fluorescence spectra and fluorescence quantum yield were measured using a Horiba FluoroMax-4 spectrophotometer at room temperature. The phosphorescence spectra were obtained by a Hitachi F7000 spectrophotometer at 77 K. The transient photoluminescence decay profiles of the dendrimers in film state were recorded using an Edinburgh Instruments FLS980 spectrometer. The temperature dependence experiment is conducted under low temperature refrigeration system from Advanced Research Systems Company. Cyclic voltammetry was performed using a CHI660E analyzer with a scan rate of 100 mV/s in MeCN solution at room temperature. A platinum plate as the working electrode, a Pt-wire counter electrode, and a saturated calomel electrode (SCE) as the reference electrode were used. The supporting electrolyte was tetrabutylammonium hexafluorophosphate (0.1 M) and ferrocene was selected as the internal standard. Thermogravimetric analysis (TGA) of the compounds was conducted on a Setaram thermogravimetric analyzer at a heating rate of 10 °C/min under nitrogen atmosphere. Differential scanning calorimetry (DSC) measurements were performed at both heating and cooling rates of 5 °C/min under nitrogen atmosphere, using DSC Q100 V9.4 Build 287 apparatus.

2.3. OLED fabrication and characterization

Patterned glass substrates coated with indium tin oxide (ITO) ($20 \Omega \text{ square}^{-1}$) were cleaned by a surfactant scrub, washed successively with deionized water, acetone and isopropanol in an ultrasonic bath, and then dried at 120 °C in a heating chamber for 8 h. A 30-nm-thick poly(3,4-ethylenedioxythiophene): poly(styrenesulfonic acid) (PEDOT:PSS) hole injection layer was spin-coated on top of ITO and baked at 120 °C for 20 min. Thin films (45 nm thick) of the dendrimers as the emitting layer were deposited on top of the PEDOT:PSS layer by spin-coating the chlorobenzene solution of **G2** or **G3**. Then an electron-transporting layer of 1,3,5-tris(*N*-phenylbenzimidazol-2-yl)benzene (TPBI, 30 nm) and LiF (1 nm) and Al (100 nm) as the cathode were deposited by vacuum evaporation under a base pressure of 5×10^{-4} Pa. The EL spectra and CIE coordinates were measured with a PR-655 spectra colorimeter. The current-voltage-forward luminance curves were measured using a Keithley 2400 source meter and a calibrated silicon photodiode. All the measurements were carried out at room temperature under ambient conditions.

2.4. DFT calculation

Geometry optimization for the dendrimers was carried out using Gaussian 03. The results were obtained by DFT calculation using B3LYP functional and the 6-31G (d, p) basis. The molecular orbitals were visualized using Gaussview.

2.5. Synthetic procedures

2.5.1. 3,6-Di-*tert*-butylcarbazole (**D1**)

Carbazole (5.016 g, 30 mmol) and AlCl_3 (4.0 g, 30 mmol) were suspended in CH_2Cl_2 (120 mL). After cooled to 0 °C, *tert*-butyl chloride (7.5 ml 60 mmol) in CH_2Cl_2 (20 mL) was added dropwise over 20 min to give a dark yellow solution. The mixture was stirred at 0 °C for 1 h, at room temperature for 9 h, and then poured into ice water and extracted with CH_2Cl_2 . The combined organic phase was washed with water, brine, dried over anhydrous MgSO_4 , filtered, and concentrated under reduced pressure. The crude product was purified by recrystallization (CH_2Cl_2 /petroleum ether) to give **D1** as a white solid (5.03 g, 60%). ^1H NMR (600 MHz, CDCl_3): δ 8.07 (d, $J = 1.8$ Hz, 2H), 7.85 (s, 1H), 7.46 (dd, $J = 8.4, 1.8$ Hz, 2H), 7.33 (d, $J = 8.4$ Hz, 2H), 1.45 (s, 18H).

2.5.2. 3,6-Diiodocarbazole (**1**)

Carbazole (1.00 g, 5.98 mmol) was dissolved into acetic acid (16 mL) and the solution was heated to 50 °C. Then finely-crushed KI (1.29 g, 7.77 mmol) was added. After a few minutes of stirring, KIO₃ (1.279 g, 5.98 mmol) in acetic acid (2 mL) was added dropwise. The mixture was refluxed for 1 h to give a light red suspension. After cooling to room temperature, water was added and the mixture was extracted with CH₂Cl₂. The combined organic phase was washed with water, brine, dried over anhydrous MgSO₄, filtered, and concentrated. Purification by recrystallization (ethyl acetate/petroleum ether) gave **1** as a red-brown powder (1.61 g, 63%). ¹H NMR (600 MHz, CDCl₃): δ 8.32 (d, *J* = 1.8 Hz, 2H), 8.10 (s, 1H), 7.68 (dd, *J* = 8.4, 1.8 Hz, 2H), 7.22 (d, *J* = 8.4 Hz, 2H).

2.5.3. 3,6-Diiodo-*N*-tosylcarbazole (**2**)

To a solution of **1** (1.5 g, 3.58 mmol) and KOH (0.92 g, 16.4 mmol) in acetone (20 mL) was added slowly a solution of *p*-toluenesulfonylchloride (3.127 g, 16.4 mmol) in acetone (2 mL). The reaction mixture was reflux for 15 min, then poured into water and extracted with CH₂Cl₂. The combined organic phase was washed with water, brine, dried over anhydrous MgSO₄, filtered, and concentrated. Purification by recrystallization (CH₂Cl₂/petroleum ether) gave **2** as a yellow solid (1.44 g, 70%). ¹H NMR (600 MHz, CDCl₃): δ 8.17 (d, *J* = 1.2 Hz, 2H), 8.07 (d, *J* = 9.0 Hz, 2H), 7.78 (dd, *J* = 9.0, 1.8 Hz, 2H), 7.65 (d, *J* = 8.4 Hz, 2H), 7.13 (d, *J* = 7.8 Hz, 2H), 2.29 (s, 3H).

2.5.4. 3,6-Bis(3,6-di-*tert*-butylcarbazol-*N*-yl)-*N*-tosylcarbazole (**3**)

CuI (0.29 g, 1.5 mmol), K₃PO₄ (1.592 g, 7.5 mmol), and (±)-*trans*-1,2-diaminocyclohexane (**DACH**, 0.2 mL, 1.6 mmol) were added to a solution of **2** (1.72 g, 3 mmol) and **D1** (1.85 g, 6.6 mmol) in toluene (40 mL). The mixture was stirred at reflux for 24 h. After cooling to

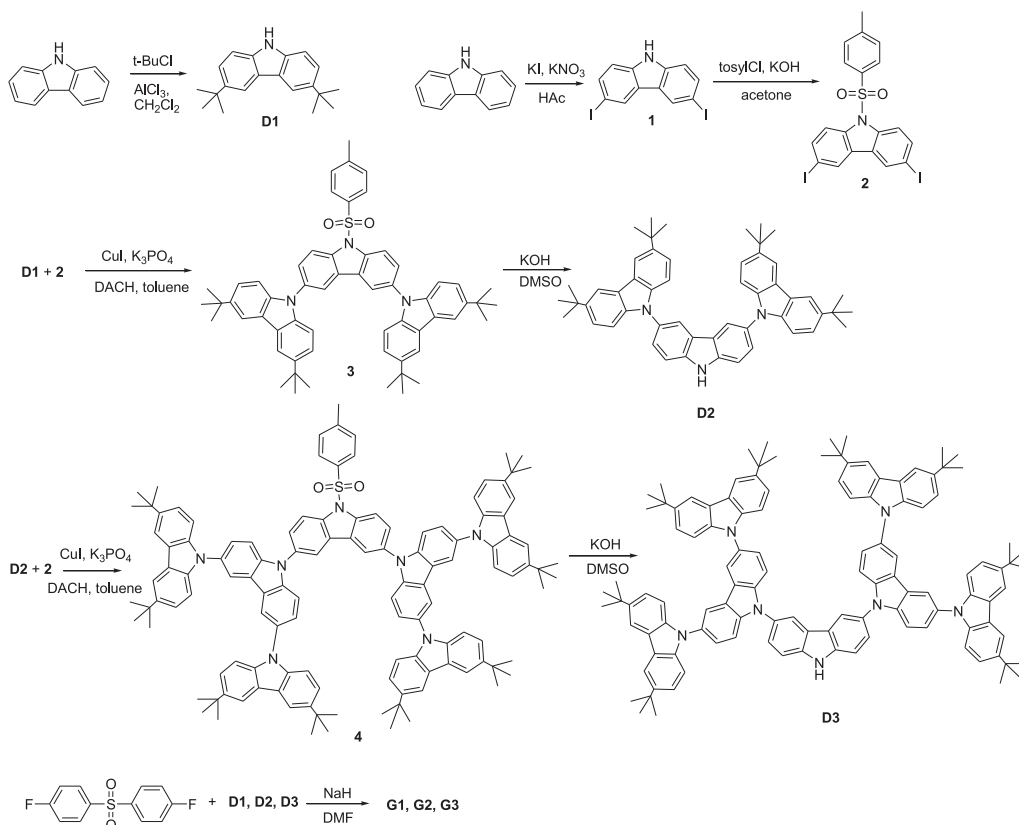
room temperature, water was added and the mixture was extracted with CH₂Cl₂. The combined organic phase was washed with water, brine, dried over anhydrous MgSO₄, filtered, and concentrated. Purification by column chromatography over silica gel (eluent: CH₂Cl₂/petroleum ether 1:4) gave **3** as a white solid (1.18 g, 45%). ¹H NMR (600 MHz, CDCl₃): δ 8.56 (d, *J* = 8.4 Hz, 2H), 8.14 (d, *J* = 1.8 Hz, 4H), 8.04 (d, *J* = 1.8 Hz, 2H), 7.92 (d, *J* = 8.4 Hz, 2H), 7.73 (dd, *J* = 9.0, 1.8 Hz, 2H), 7.44 (dd, *J* = 9.0, 1.8 Hz, 4H), 7.29–7.33 (m, 6H), 2.40 (s, 3H), 1.45 (s, 36H).

2.5.5. 3,6-Bis(3,6-di-*tert*-butylcarbazol-*N*-yl)carbazole (**D2**)

To a solution of **3** (1.0 g, 1.14 mmol) in DMSO (6 mL)-THF (12 mL)-water (2 mL) was added powdered KOH (0.13 g, 2.32 mmol). The mixture was stirred at reflux for 1.5 h. After cooling to room temperature, 10% HCl (20 mL) was added followed by water (10 mL) and methanol (5 mL). The precipitate was collected by filtration and washed with water. The crude product was recrystallized (CH₂Cl₂/methanol) to give **D2** as a white solid (0.82 g, 99%). ¹H NMR (600 MHz, CDCl₃): δ 8.40 (s, 1H), 8.17 (dd, *J* = 4.8, 1.8 Hz, 6H), 7.66 (d, *J* = 8.4 Hz, 2H), 7.60 (dd, *J* = 8.4, 1.8 Hz, 2H), 7.45 (dd, *J* = 8.4, 1.8 Hz, 4H), 7.13 (d, *J* = 8.4 Hz, 4H), 1.46 (s, 36H).

2.5.6. 3,6-Bis[3,6-bis(3,6-di-*tert*-butylcarbazol-*N*-yl)carbazol-*N*-yl]-*N*-tosylcarbazole (**4**)

Following the procedure for the synthesis of **3**, **2** (1.15 g, 2 mmol), **D2** (3.26 g, 4.5 mmol), CuI (191 mg, 1 mmol), K₃PO₄ (1.06 g, 5 mmol), (±)-*trans*-1,2-diaminocyclohexane (0.15 mL, 1.2 mmol) were heated at reflux for 36 h. The mixture was purified by column chromatography over silica gel (eluent: CH₂Cl₂/petroleum ether 1:4–1:2) to yield **4** as a light pink solid (1.41 g, 40%). ¹H NMR (600 MHz, CDCl₃): δ 8.96 (s, 2H), 8.81 (d, *J* = 12.6 Hz, 6H), 8.29 (s, 8H), 8.10 (m, 4H), 7.71 (d, *J* = 8.4 Hz, 4H), 7.66 (d, *J* = 8.4 Hz, 4H),



Scheme 2. Synthesis of the dendrimers.

7.50 (d, $J = 8.4$ Hz, 2H), 7.44 (d, $J = 7.8$ Hz, 8H), 7.30 (d, $J = 9$ Hz, 8H), 2.37 (s, 3H), 1.39 (s, 72H).

2.5.7. 3,6-Bis[3,6-bis(3,6-di-tert-butylcarbazol-N-yl)carbazol-N-yl]carbazole (**D3**)

Following the procedure for the synthesis of **D2**, **4** (881 mg, 0.5 mmol) and KOH (68 mg, 1.2 mmol) were treated at reflux for 1.5 h. **D3** was obtained by recrystallization ($\text{CH}_2\text{Cl}_2/\text{methanol}$) as a white solid (788 mg, 99%). $^1\text{H NMR}$ (600 MHz, $\text{DMSO}-d_6$) δ 10.03 (s, 1H), 8.81 (d, $J = 1.2$ Hz, 2H), 8.68 (s, 4H), 8.29 (dd, $J = 8.4, 1.8$ Hz, 8H), 7.97 (d, $J = 8.4$ Hz, 2H), 7.92 (dd, $J = 7.8, 1.2$ Hz, 2H), 7.88 (dd, $J = 8.4, 1.8$ Hz, 2H), 7.70 (d, $J = 7.8$ Hz, 2H), 7.67 (d, $J = 1.9$ Hz, 4H), 7.46 (dd, $J = 8.4, 1.8$ Hz, 8H), 7.32 (d, $J = 8.4$ Hz, 8H), 1.40 (s, 72H).

2.5.8. General synthetic procedure for the dendrimers

To a solution of the dendron (2.2 mmol) in dry dimethylformamide (DMF) (5 mL) was added a solution of sodium hydride (96 mg, 4 mmol) in dry DMF (6 mL). After the solution was stirred at room temperature for 30 min, bis(*p*-fluorophenyl) sulfone (254 mg, 1 mmol) in dry DMF (5 mL) was added, and the mixture was stirred at 100 °C for an additional 7 h. After cooling to room temperature, the mixture was poured into ice water (100 mL) and filtered. The crude product was purified by recrystallization or by column chromatography to give the dendrimers.

2.5.8.1. Bis(4-(3,6-di-tert-butylcarbazole)phenyl) sulfone (**G1**). **G1** was obtained from **D1** (615 mg) and recrystallized from ethanol as white crystals (400 mg, 52%). $^1\text{H NMR}$ (600 MHz, CDCl_3): δ 8.24 (dd, $J = 7.2, 1.8$ Hz, 4H), 8.13 (d, $J = 2.4$ Hz, 4H), 7.82 (dd, $J = 6.6, 1.8$ Hz, 4H), 7.49–7.44 (m, 8H), 1.46 (s, 36H).

2.5.8.2. Bis(4-(3,6-bis(3,6-di-tert-butylcarbazol-N-yl)carbazole)phenyl) sulfone (**G2**). **G2** was obtained from **D2** (1.589 g) and recrystallized from ethanol as white crystals 794 mg, 48%). $^1\text{H NMR}$

(600 MHz, CDCl_3): δ 8.43 (dd, $J = 7.2, 1.8$ Hz, 4H), 8.24 (d, $J = 1.8$ Hz, 4H), 8.15 (d, $J = 2.4$ Hz, 8H), 8.04 (dd, $J = 7.2, 1.8$ Hz, 4H), 7.74 (d, $J = 9.0$ Hz, 4H), 7.45 (dd, $J = 8.4, 1.8$ Hz, 4H), 7.35 (dd, $J = 8.4, 1.8$ Hz, 8H), 7.32 (d, $J = 9.0$ Hz, 8H), 1.45 (s, 72H); $^{13}\text{C NMR}$ (600 MHz, CDCl_3) δ 146.7, 146.3, 143.1, 142.9, 142.4, 134.9, 133.1, 130.4, 129.2, 127.6, 126.6, 126.2, 122.4, 121.2, 113.9, 111.9, 37.7, 35.0; MALDI TOF-MS: m/z 1674.91 $[\text{M}+\text{NH}_4]^+$; Anal. Calcd for $\text{C}_{118}\text{H}_{120}\text{N}_6\text{O}_2\text{S}$: C, 84.04, H, 7.17, N, 4.98; Found: C, 82.70, H, 7.26, N, 4.64.

2.5.8.3. Bis(4-(3,6-bis(3,6-bis(3,6-di-tert-butylcarbazol-N-yl)carbazol-N-yl)carbazole)phenyl) sulfone (**G3**). **G3** was obtained from **D3** (3.535 g) and recrystallized from methanol followed by column chromatography over silica gel (eluent: $\text{CH}_2\text{Cl}_2/\text{petroleum ether}$ 1:2) as white crystals (1.575 g). $^1\text{H NMR}$ (600 MHz, CDCl_3) δ 8.56 (q, 4H), 8.26 (d, $J = 1.2$ Hz, 8H), 8.68 (d, $J = 9.0$ Hz, 20H), 7.61 (q, 16H), 7.43 (m, 20H), 7.32 (m, 16H), 1.44 (s, 144H). $^{13}\text{C NMR}$ (600 MHz, CDCl_3) δ 142.6, 141.2, 140.2, 131.0, 126.1, 123.9, 123.5, 123.1, 119.5, 116.2, 110.9, 109.0, 34.706, 32.021; MALDI TOF-MS: m/z 3451.25 $[\text{M}+\text{Na}]^+$; Anal. Calcd for $\text{C}_{246}\text{H}_{240}\text{N}_{14}\text{O}_2\text{S}$: C, 85.48, H, 7.00, N, 5.67; Found: C, 83.53, H, 6.88, N, 5.14.

3. Results and discussion

3.1. Synthesis of the dendrimers

The synthetic routes of the dendrimers were shown in Scheme 2. The carbazole-based dendrons were synthesized according to the literature using tosyl groups to protect the carbazole nitrogen atoms [24]. Dendrimers **G1**, **G2** and **G3** with diphenyl sulfone core were synthesized through a catalyst-free aromatic nucleophilic substitution reaction between the corresponding dendrons and bis(4-fluorophenyl)sulfone at moderate yields of 40–52%, respectively. All of the new compounds were characterized by NMR spectroscopy, MALDI-TOF mass spectroscopy, and elemental

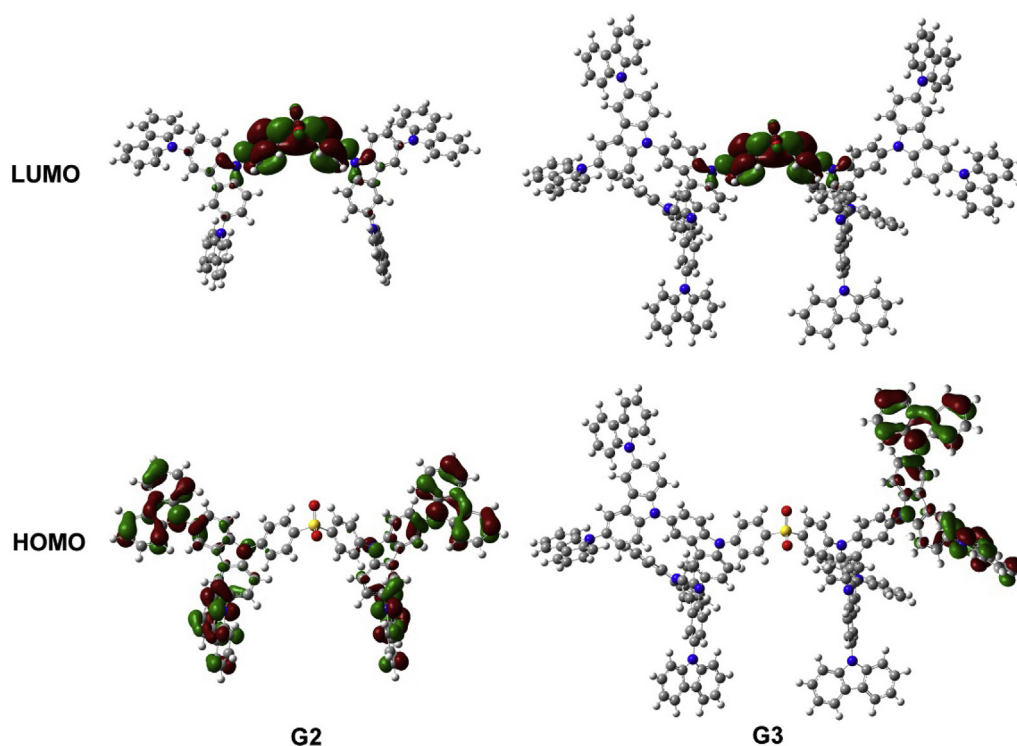


Fig. 1. The spatial distributions of (bottom) HOMO and (top) LUMO energy densities of **G2** and **G3** by DFT B3LYP/6-31G(d) calculation.

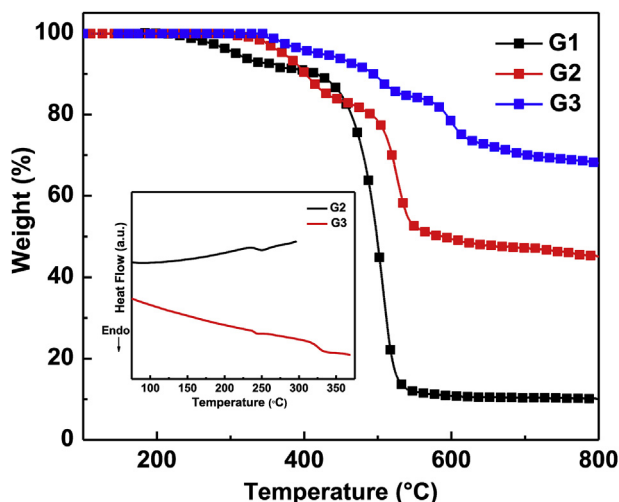


Fig. 2. TGA thermograms and DSC traces (inset) of the dendrimers (at a heating rate of 10 °C/min).

analysis. The target compounds **G1**, **G2** and **G3** exhibited good solubility in common solvents such as toluene, chloroform and tetrahydrofuran, thus they can be purified by column chromatography or recrystallization, and can be applied in OLEDs through solution-process.

3.2. DFT calculation

The calculation results revealed that the molecules adopted nonplanar three-dimensional structures with carbazolyl dendrons arranging twisted around the diphenyl sulfone core (Fig. 1). For dendrimers **G2** and **G3**, the HOMOs were mainly distributed over the outer carbazolyl units, whereas the LUMOs were delocalized on the electron-withdrawing diphenyl sulfone core. The twisted geometry, together with the effective spatial separation between the HOMO and LUMO, implied a small singlet-triplet splitting energy for the T_1 -to- S_1 transition of the molecules, which was considered to be beneficial for efficient reverse intersystem crossing (RISC) and as a result for TADF behavior.

3.3. Thermal stabilities

The thermal properties of the dendrimers were investigated by means of thermal gravimetric analyses (TGA) and differential scanning calorimetry (DSC) (Fig. 2), and the data was listed in Table 1. The dendrimers exhibited high thermal stability with decomposition temperatures (T_d , corresponding to 5% weight loss) in the range of 311–425 °C. Their thermal stability increased with the increase of the generation, probably owing to the increased number of the thermal-stabilized carbazole groups. The

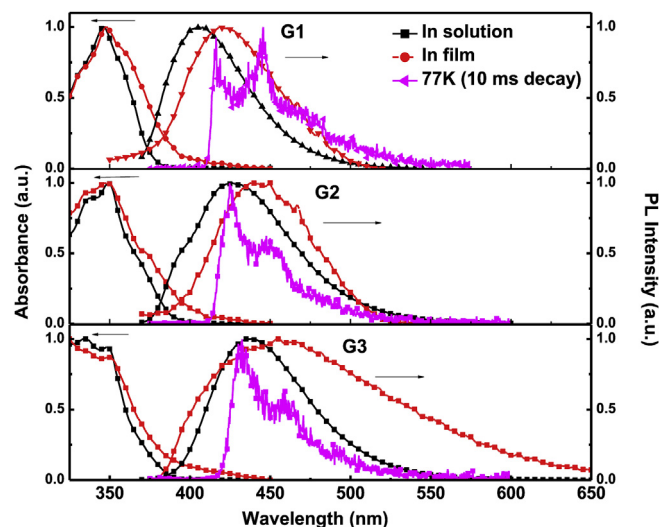


Fig. 3. UV-vis absorption and PL spectra of dendrimers **G1**–**G3** in dilution solution of toluene (10^{-5} M) and in solid film, and their phosphorescence spectra (delayed by 10 ms) in toluene at 77 K.

morphology stabilities of **G2** and **G3** were confirmed by DSC, from which no obvious phase transition peaks were observed, and only an endothermic step due to the glass transition was detected at 242 and 325 °C for **G2** and **G3**, respectively. The increased glass transition temperature (T_g) from **G2** to **G3** can be attributable to their increased size of the bulky carbazole dendrons. The good thermal and morphological stability of **G2** and **G3** suggested that homogeneous and amorphous thin films could be prepared through solution processing, which is expected for application in OLEDs.

3.4. Photophysical properties

3.4.1. Steady-state photoluminescence

The UV-vis absorption and photoluminescence (PL) spectra of the dendrimers in toluene were shown in Fig. 3. All the dendrimers showed an intramolecular charge-transfer (ICT) absorption band around 347 nm, indicating that the ICT character of the molecules remained with the increase of the dendrimer generation. The ICT characters of the dendrimers were further demonstrated by the PL spectra in various solvents from nonpolar solvent toluene to polar solvent dichlorobenzene (Fig. S1, Supplementary material). Broad and unstructured emission bands with the emission peaks shifted distinctly by changing the polarity of the solvent could be observed. The effect of solvent polarity on the excited state was analyzed using the Lippert-Mataga relationship (Eq. S(1), Supplementary material), and all of the dendrimers exhibited positive solvatochromism with emission maxima depending approximately linearly on the solvent polarity, indicating the ICT behavior of the dendrimers.

Table 1

Physical properties of the dendrimers.

Compound	Solution		Film		E_g^a (eV)	S_1/T_1^b (eV)	ΔE_{ST} (eV)	τ_p (ns)	τ_d (μ s)	HOMO/LUMO ^c (eV)	T_g/T_d (°C)
	$\lambda_{UV}/\lambda_{PL}$ (nm)	Φ_{Air}/Φ_{N2} (%)	$\lambda_{UV}/\lambda_{PL}$ (nm)	Φ_{Air}/Φ_{N2} (%)							
G1	346/406	53/60	347/421	23/42	3.2	3.34/3.01	0.33	7.6	540/2600	−5.80/−2.60	−/311
G2	348/426	53/64	347/438	34/58	3.1	3.25/3.00	0.25	6.5	347/2530	−5.74/−2.64	242/372
G3	349/439	44/52	349/451	15/22	3.2	3.15/2.98	0.17	8.7	378/2860	−5.70/−2.50	325/425

^a Calculated from the absorption spectra threshold, $E_g = 1240/\lambda$.

^b Calculated from the onset of the fluorescence (for S_1) and phosphorescence (for T_1) spectra.

^c Estimated with reference to ferrocene (4.8 eV); LUMO = HOMO + E_g .

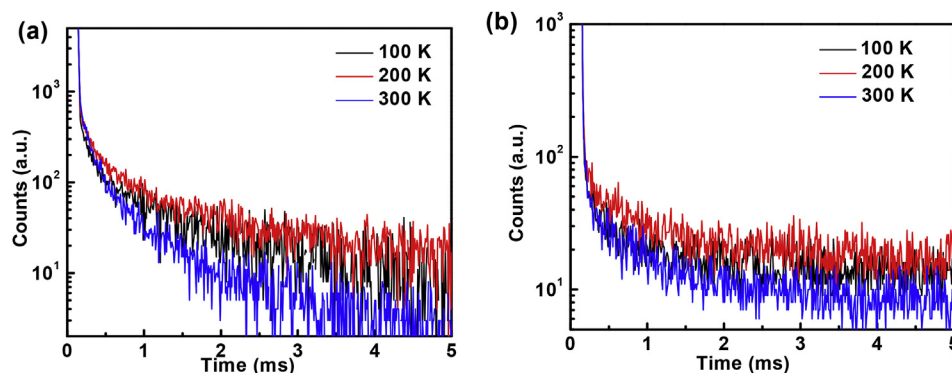


Fig. 4. Temperature-dependence of the transient PL spectra for (a) 5 wt% **G2** and (b) 5 wt% **G3** doped in PMMA.

In toluene solution, the maximum PL wavelength showed a bathochromic shift from **G1** at 406 nm to **G3** at 439 nm with the increase of the dendrimer generation. The lowered S_1 energy may be derived from the increased distance between the donor (outer carbazole) and the acceptor (diphenyl sulfone) from **G1** to **G3** [20,25]. In films, no obvious bathochromic shifts were detected in the UV–vis absorption spectra of the dendrimers, and a bathochromic shift of 15, 15 and 12 nm in the PL spectra with respect to that in toluene solution was observed for **G1**, **G2** and **G3**, respectively. The small bathochromic effect implied that the intermolecular interactions could be effectively prevented in the solid state due to the bulky carbazole dendrons.

In contrast to their fluorescence spectra with strong CT characters, the phosphorescence spectra of the dendrimers measured at 77 K with 10 ms decay showed well-resolved vibrational structures, indicating their T_1 states were locally excited triplet states (3LE) [12]. The onset of the fluorescence spectrum and that of the highest energy peak of the phosphorescence spectrum were used to determine the zero-zero energies (E_{0-0}) of the 1CT and 3LE states, respectively, and the energy levels E_{0-0} were listed in Table 1. It is noted that the T_1 levels of the dendrimers are quite similar to each other (~ 3.0 eV), implying that by attaching higher generation carbazoles via their N-position to the 3,6-positions of the inner carbazole moiety does not influence on the triplet energy of the whole molecule [24]. With the decreased S_1 energies from **G1** to **G3**, the ΔE_{ST} values of the molecules decreased with the increase of the dendron generation from 0.33 eV for **G1** to 0.17 eV for **G3**. In addition, the fluorescence quantum yield (Φ_f) values of the

dendrimers in both solution and neat film exhibited enhancement under N_2 atmosphere with respect to those in air condition, which suggested that an effective up-conversion of the triplet excitons did occur when oxygen was excluded.

3.4.2. Time-resolved fluorescence decays

To further demonstrate that TADF occurred in the solid state, **G2**- and **G3**-doped PMMA films (5 ± 1 wt %) were investigated. The transient PL decay characteristics and temperature dependence were measured under vacuum (Fig. 4). The signals displayed a fast decay and a slower one with their spectra showing good overlap from each other, which can be assigned to the prompt and delayed fluorescence, respectively (Table 1, and Fig. S2, Supplementary material). Moreover, the intensity of the delayed component increased with the temperature from 100 K to 200 K, implying the TADF mechanism of the delayed fluorescence. Interestingly, the intensity of the delayed component slightly dropped with increasing the temperature from 200 to 300 K, suggesting a slight increase in non-radiative processes through vibration or molecular interactions over 200 K [26]. At 300 K, the lifetimes were estimated to be 464 μs for **G2** and 814 μs for **G3**, respectively. It is noted that **G3** has a smaller ΔE_{ST} but a longer lifetime, which might be attributable to the slower radioactive rate constant (k_F and k_{TADF}) of **G3** because of the lower fluorescent quantum yield (Table S1, Supplementary material) [27].

3.5. Electrochemical properties

The electrochemical characteristics of the dendrimers were measured by cyclic voltammetry. Dendrimers **G1** to **G3** exhibited reversible oxidation processes upon the anodic sweep. The first oxidation waves of the dendrimers shifted to lower potentials with increasing the dendrimer generation from **G1** at 1.43 V to **G3** at 1.31 V, owing to the extended conjugation of the dendrons and the increased electron-donating ability with increasing the dendron generation. The HOMO levels of dendrimers **G1** to **G3** determined from the onsets of the oxidation potentials were -5.80 , -5.73 and -5.68 eV, respectively, by assuming the energy level of Fc/Fc^+ to be 4.8 eV below the vacuum level. No reduction signals were detected for any of the compounds. Thus the LUMO levels of the dendrimers were calculated from the HOMO levels and the corresponding optical bandgaps (E_g s) (Table 1) (See Fig. 5).

3.6. Electroluminescent properties

Considering the neat films of **G2** and **G3** exhibited favorable properties, to further investigate their electroluminescent (EL) performance, double-layer solution-processed OLEDs were

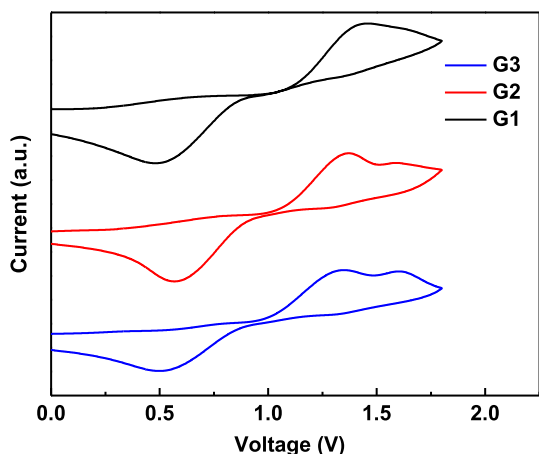


Fig. 5. CV curves of dendrimers **G1**–**G3** in CH_2Cl_2 or MeCN solution using 0.1 M Bu_4NPF_6 at a scan rate of 100 mV/s.

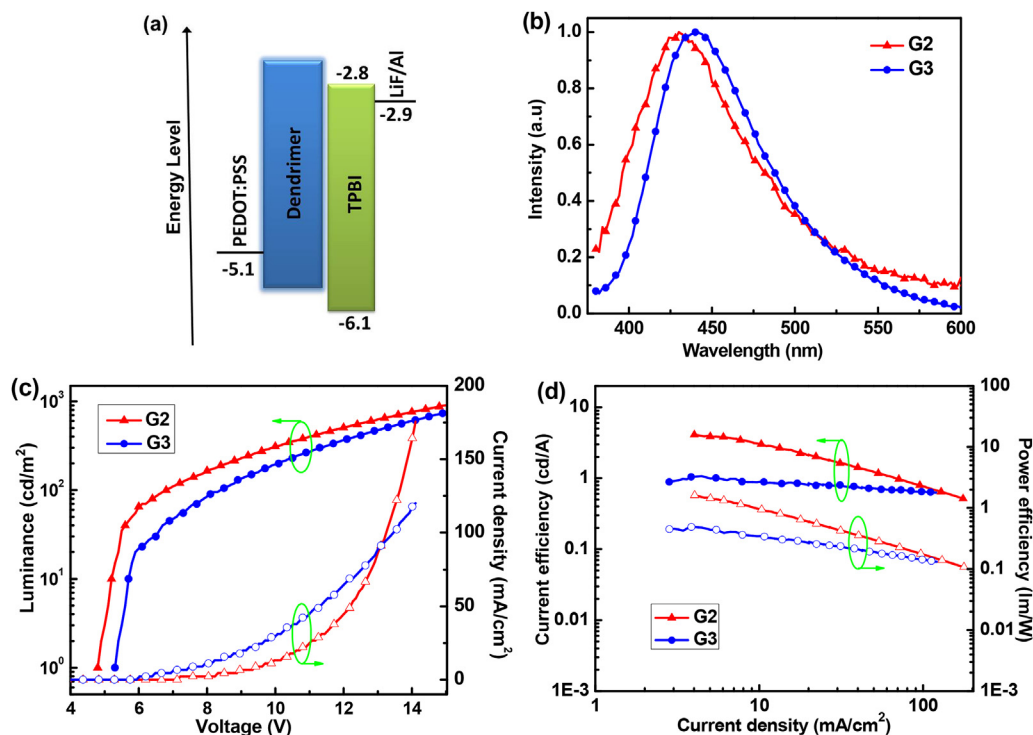


Fig. 6. (a) Energy level diagrams, (b) EL spectra, (c) Current density–voltage–luminance and (d) Current efficiency–current density–power efficiency characteristics of the OLEDs.

Table 2

EL performance of the OLEDs.

Device	V_{on}^a (V)	CE_{max} (cd A ⁻¹) ^b	PE_{max} (lm W ⁻¹) ^c	PE_{fmax}/PE_{max} (%) ^d	CIE (x,y) ^e
G2	4.8	4.1	1.6	14	(0.15, 0.12)
G3	5.2	1.07	0.49	56	(0.19, 0.15)

^a Turn-on voltage (at 1 cd m⁻²).

^b The maximum current efficiency.

^c The maximum power efficiency.

^d The PE value at the maximum current density vs the peak value.

^e At the driving voltage of 12 V.

fabricated with the structure of ITO/PEDOT:PSS (30 nm)/EML (45 nm)/TPBI (30 nm)/LiF (1 nm)/Al (100 nm), in which **G2** and **G3** were employed as the nondoped emitting layers, respectively. The energy levels and the electroluminescent characteristics of the devices were shown in Fig. 6 and Table 2. For comparison, **G1** was also applied as the non-doped emitter for the control device (Fig. S3, Supplementary material). The OLEDs exhibited deep-blue and true blue emission with λ_{max} s at 428 and 440 nm, and CIE coordinates at (0.15, 0.12) and (0.19, 0.15), respectively (Fig. 6b). The EL spectra of both two devices were almost identical to their corresponding PL spectra in toluene solutions (Fig. S4, Supplementary material). Both of the two devices displayed low turn-on voltages at about 5 V, which could be attributable to the high-lying HOMO levels and as a result a small energy barrier at the PEDOT:PSS/dendrimer interface. The **G2** device achieved a better performance with a maximum current efficiency (CE_{max}) of 4.1 cd/A and a maximum power efficiency (PE_{max}) of 1.6 lm/W. As shown in Fig. 6d and Fig. S3b, compared with the control device, the efficiencies of both devices decreased quite slowly with increasing current density. Remarkably, the power efficiency of **G3** device at the maximum current density was as high as 56% respects to the PE_{max} , suggesting the triplet-singlet and triplet-triplet annihilation rate could be reduced with the reduction of ΔE_{ST} and the inhibited intermolecular interactions by introducing carbazole dendrons. The satisfying EL

property of **G2** well demonstrated our design on TADF dendrimers for molecular modification, i.e., smaller ΔE_{ST} , weak intermolecular interactions, good film forming ability (Fig. S5, Supplementary material), as well as balanced charge transport ability.

4. Conclusion

In conclusion, two TADF dendrimers **G2** and **G3** based on bis[4-(3,6-di-*tert*-butylcarbazole)phenyl]sulfone (**G1**) core incorporating carbazole dendrons were developed. These dendrimer emitters inherited blue emitting and similar triplet energy level to the parent **G1**, but superior in smaller ΔE_{ST} to facilitate the RISC process, inhibited intermolecular interactions, higher thermal and amorphous stabilities and good solution processability. Solution-processed OLED by employing dendrimer **G2** as the non-doped emissive layer achieved deep blue with a maximum current efficiency of 4.1 cd/A and a CIE coordinate at (0.15, 0.12). Similar device based on **G3** emitting layer displayed negligible efficiency roll-off at high current density. These results pave a way for the molecular modification on adjusting ΔE_{ST} for the TADF emitters, and the deep-blue TADF dendrimers could be promising candidates for applications in solution-processable OLEDs.

Acknowledgements

This work was financially supported by the National Natural Science Foundation of China (61605138, 61205179, 61307030, 61307029, 51503022), the “Program for New Century Excellent Talents (NCET) in University” (NCET-13-0927), the Qualified Personnel Foundation of Taiyuan University of Technology (QPFT) (No:tyutrc-201255a), and the Shanxi Provincial Key Innovative Research Team in Science and Technology (201513002-10), Open Foundation of State Key Laboratory of Electronic Thin Films and Integrated Devices (KFJJ201507), Basic and Frontier Research Program of Chongqing Municipality (cstc2015jcyjA50036), Natural Science Foundation of Yongchuan District (Ycstc,2015nc4001).

Appendix A. Supplementary data

Supplementary data related to this article can be found at <http://dx.doi.org/10.1016/j.dyepig.2017.01.036>.

References

- [1] Xiao L, Chen Z, Qu B, Luo J, Kong S, Gong Q, et al. Recent progresses on materials for electrophosphorescent organic light-emitting devices. *Adv Mater* 2011;23:926–52.
- [2] Gather MC, Kohnen A, Meerholz K. White organic light-emitting diodes. *Adv Mater* 2011;23:233–48.
- [3] Yook KS, Lee JY. Organic materials for deep blue phosphorescent organic light-emitting diodes. *Adv Mater* 2012;24:3169–90.
- [4] Kumar S, Singh M, Jou JH, Ghosh S. Trend breaking substitution pattern of phenothiazine with acceptors as a rational design platform for blue emitters. *J Mater Chem C* 2016;4:6769–77.
- [5] Zhang J, Li J, Chen W, Zheng D, Yu J, Wang H, et al. An efficient blue thermally activated delayed fluorescence material based on 4-fluorocyanobenzene derivative for organic light-emitting diodes. *Tetrahedron Lett* 2016;57:2044–8.
- [6] Li C, Wei J, Han J, Li Z, Song X, Zhang Z, et al. Efficient deep-blue OLEDs based on phenanthro[9,10-d]imidazole-containing emitters with AIE and bipolar transporting properties. *J Mater Chem C* 2016;4:10120–9.
- [7] Zhao L, Wang S, Shao S, Ding J, Wang L, Jing X, et al. Stable and efficient deep-blue terfluorenes functionalized with carbazole dendrons for solution-processed organic light-emitting diodes. *J Mater Chem C* 2015;3:8895–903.
- [8] He C, Guo H, Peng Q, Dong S, Li F. Asymmetrically twisted anthracene derivatives as highly efficient deep-blue emitters for organic light-emitting diodes. *J Mater Chem C* 2015;3:9942–7.
- [9] Uoyama H, Goushi K, Shizu K, Nomura H, Adachi C. Highly efficient organic light-emitting diodes from delayed fluorescence. *Nature* 2012;492:234–8.
- [10] Hirata S, Sakai Y, Masui K, Tanaka H, Lee SY, Nomura H, et al. Highly efficient blue electroluminescence based on thermally activated delayed fluorescence. *Nat Mater* 2015;14:330–6.
- [11] Zhang Q, Li B, Huang S, Nomura H, Tanaka H, Adachi C. Efficient blue organic light-emitting diodes employing thermally activated delayed fluorescence. *Nat Phot* 2014;8:326–32.
- [12] Zhang Q, Li J, Shizu K, Huang S, Hirata S, Miyazaki H, et al. Design of efficient thermally activated delayed fluorescence materials for pure blue organic light emitting diodes. *J Am Chem Soc* 2012;134:14706–9.
- [13] Wu S, Aonuma M, Zhang Q, Huang S, Nakagawa T, Kuwabara K, et al. High-efficiency deep-blue organic light-emitting diodes based on a thermally activated delayed fluorescence emitter. *J Mater Chem C* 2014;2:421–4.
- [14] Wang H, Xie L, Peng Q, Meng L, Wang Y, Yi Y, et al. Novel thermally activated delayed fluorescence materials—thioxanthone derivatives and their applications for highly efficient OLEDs. *Adv Mater* 2014;26:5198–204.
- [15] Huang B, Qi Q, Jiang W, Tang J, Liu Y, Fan W, et al. Thermally activated delayed fluorescence materials based on 3,6-ditert-butyl-9-((phenylsulfonyl)phenyl)-9H-carbazoles. *Dyes Pigm*. 2014;111:135–44.
- [16] Mei L, Hu J, Cao X, Wang F, Zheng C, Tao Y, et al. The inductive-effect of electron withdrawing trifluoromethyl for thermally activated delayed fluorescence: tunable emission from tetra- to penta-carbazole in solution processed blue OLEDs. *Chem Comm* 2015;51:13024–7.
- [17] Hu J, Pu Y, Satoh F, Kawata S, Katagiri H, Sasabe H, et al. Bisanthracene-based donor–acceptor-type light-emitting dopants: highly efficient deep-blue emission in organic light-emitting devices. *Adv Funct Mater* 2014;24:2064–71.
- [18] Jiang Y, Wang L, Zhou Y, Cui Y, Wang J, Cao Y, et al. π -Conjugated dendrimers as stable pure-blue emissive materials: photophysical, electrochemical, and electroluminescent properties. *Chem Asian J* 2009;4:548–53.
- [19] Li J, Liu D. Dendrimers for organic light-emitting diodes. *J Mater Chem* 2009;19:7584–91.
- [20] Albrecht K, Matsuoka K, Fujita K, Yamamoto K. Carbazole dendrimers as solution-processable thermally activated delayed-fluorescence materials. *Angew Chem Int Ed* 2015;54:5677–82.
- [21] Luo J, Gong S, Gu Y, Chen T, Li Y, Zhong C, et al. Multi-carbazole encapsulation as a simple strategy for the construction of solution-processed, non-doped thermally activated delayed fluorescence emitters. *J Mater Chem C* 2016;4:2442–6.
- [22] Li Y, Xie G, Gong S, Wu K, Yang C. Dendronized delayed fluorescence emitters for non-doped, solution-processed organic light-emitting diodes with high efficiency and low efficiency roll-off simultaneously: two parallel emissive channels. *Chem Sci* 2016;7:5441–7.
- [23] Ban X, Jiang W, Lu T, Jing X, Tang Q, Huang S, et al. Self-host thermally activated delayed fluorescent dendrimers with flexible chains: an effective strategy for non-doped electroluminescent devices based on solution processing. *J Mater Chem C* 2016;4:8810–6.
- [24] Li J, Zhang T, Liang Y, Yang R. Solution-processible carbazole dendrimers as host materials for highly efficient phosphorescent organic light-emitting diodes. *Adv Funct Mater* 2013;23:619–28.
- [25] Zhao Z, Jin H, Zhang Y, Shen Z, Zou D, Fan X. Synthesis and properties of dendritic emitters with a fluorinated starburst oxadiazole core and twisted carbazole dendrons. *Macromolecules* 2011;44:1405–13.
- [26] Lee J, Shizu K, Tanaka H, Nomura H, Yasuda T, Adachi C. Oxadiazole- and triazole-based highly-efficient thermally activated delayed fluorescence emitters for organic light-emitting diodes. *J Mater Chem C* 2013;1:4599–604.
- [27] Tao Y, Yuan K, Chen T, Xu P, Li H, Chen R, et al. Thermally activated delayed fluorescence materials towards the breakthrough of organoelectronics. *Adv Mater* 2014;26:7931–58.